# Channel Size Conversion of Phi29 DNA-Packaging Nanomotor for Discrimination of Single- and Double-Stranded Nucleic Acids

Jia Geng,[†,§] Shaoying Wang,[†,§] Huaming Fang,[†,§] and Peixuan Guo[†,‡,§,*]

[†]Nanobiotechnology Center, [‡]Markey Cancer Center, and [§]Department of Pharmaceutical Sciences, University of Kentucky, Lexington, Kentucky 40536, United States

ABSTRACT Nanopores have been utilized to detect the conformation and dynamics of polymers, including DNA and RNA. Biological pores are extremely reproducible at the atomic level with uniform channel sizes. The channel of the bacterial virus phi29 DNA-packaging motor is a natural conduit for the transportation of double-stranded DNA (dsDNA) and has the largest diameter among the well-studied biological channels. The larger channel facilitates translocation of dsDNA and offers more space for further channel modification and conjugation. Interestingly, the relatively large wild-type channel, which translocates dsDNA, cannot detect single-stranded nucleic acids (ssDNA or ssRNA) under the current experimental conditions. Herein, we reengineered this motor channel by removing the internal loop segment of the channel. The

modification resulted in two classes of channels. One class was the same size as the wild-type channel, while the other class had a cross-sectional area about 60% of the wild-type. This smaller channel was able to detect the real-time translocation of single-stranded nucleic acids at single-molecule level. While the wild-type connector exhibited a one-way traffic property with respect to dsDNA translocation, the loop-deleted connector was able to translocate ssDNA and ssRNA with equal competencies from both termini. This finding of size alterations in reengineered motor channels expands the potential application of the phi29 DNA-packaging motor in nanomedicine, nanobiotechnology, and high-throughput single-pore DNA sequencing.
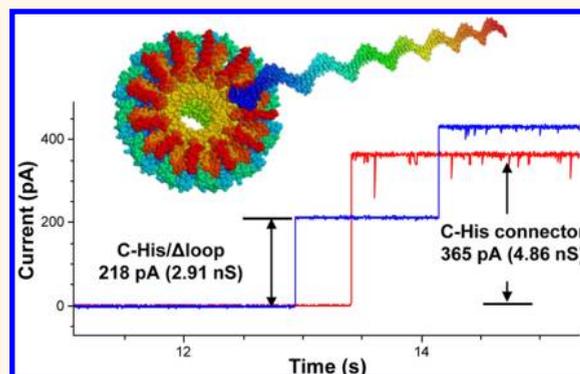
KEYWORDS: nanotechnology · nanomotor · DNA-packaging motor · bacteriophage phi29 · nanopore · sequencing · sensing

L iving systems contain a wide variety of nanomachines with diverse structures and functions. The elegant bacterial virus phi29 DNA-packaging nanomotor,[1,2] with its intricate channel[3,4] (Figure 1), has inspired its application in nanotechnology. The central core of the motor is composed of 12 copies of the gene protein gp10, which encircle to form a dodecameric channel that acts as a path for the translocation of double-stranded DNA (dsDNA) (Figure 1). The cross-sectional area of the channel is 10 nm^2 (3.6 nm in diameter) at the narrow end and 28 nm^2 (6 nm in diameter) at its wider end.[3,4] The mode of connector insertion and anchoring within the viral capsid is mediated *via* protein−protein interactions.[5,6] The connector has been inserted into a lipid bilayer, and the resulting system has been shown to exhibit robust properties

and generate extremely reliable, precise, and sensitive conductance signatures when ions or DNA pass through the channel, as revealed by single-channel conductance measurements.[7,8] Explicit engineering of the phi29 connector is possible due to its accessible crystal structure.[9,10] The pore size of the connector is nearly identical from sample to sample, and chemical conjugations within the large cavity of the pore can be made for added functionality with relative ease.[11] Furthermore, the procedures for large-scale production and purification of the connector have already been developed,[10,12−16] and anchoring within the viral capsid is mediated *via* protein−protein interactions.

The membrane-embedded connector channel has an ideal nanostructure for the detection and translocation of small molecules. Under an applied potential,
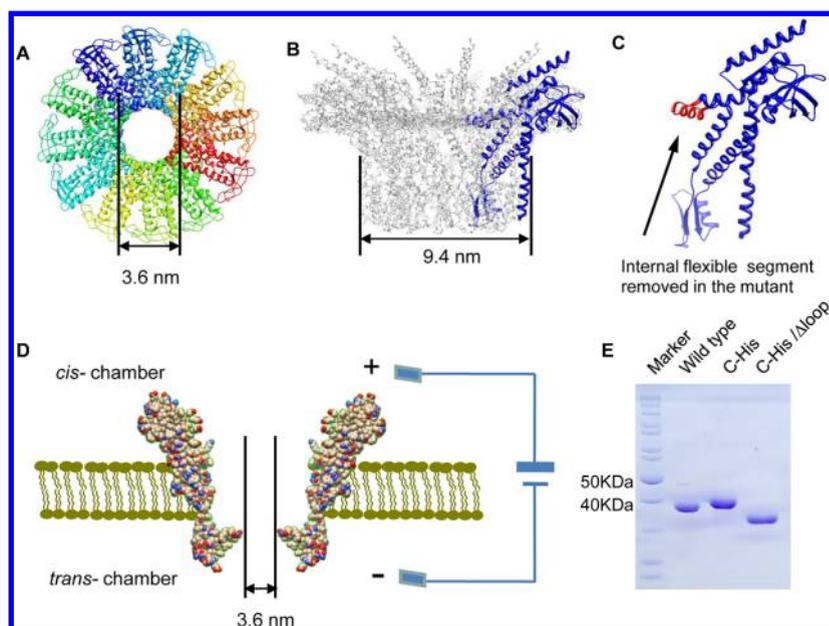
Figure 1. Illustration of phi29 DNA-packaging motor connector channel structure. (A) Top view of the connector channel with each of the dodecameric gp10 protein subunits shown in a different color. **(B)** Side view of the connector channel with an intact connector gp10 protein subunit (blue). **(C)** View of an isolated gp10 subunit with the flexible segment, which was deleted in the C-His/Δloop mutant (red). **(D)** Cross-sectional side view of the connector channel inserted into a BLM with a schematic to represent the applied voltage potential. **(E)** Polyacrylamide gel stained with Coomassie blue with lanes loaded with wild-type gp10 protein subunit, C-His gp10 protein subunit, and C-His/Δloop gp10 protein subunit. The position of the band produced by C-His gp10 protein subunit reflects a slightly larger molecular weight (MW) compared to the wild-type gp10 protein subunit, due to the addition of the 14 His residue tag. The position of the band produced by C-His/Δloop gp10 protein subunit reflects a lower MW due to the deletion of the internal flexible loop.

the translocation of dsDNA has been demonstrated extensively[7,17] by both single-channel recordings and quantitative polymerase chain reaction (PCR).[7,18−20] The translocation of dsDNA through the wild-type connector channel shows a one-way traffic property from N- to C-terminal.[18] The role of connector channel loops in late-stage DNA packaging has also been studied.[21] The connector channel acts like a one-way valve and employs a "push through one-way valve" mechanism for viral DNA packaging.[20,22] The conductance of the channel at various salt concentrations and pH environments has also been investigated.[8] The connector channel is stable over a pH range of 2 to 12, and the channel conductance demonstrates a strong linear relationship with respect to the salt concentration. The channel also exhibits gating (a transition from an open state to a closed state) at higher transmembrane potentials, a process that induces a conformational change in the channel subunits.[19]

Engineered transmembrane channels have the potential for stochastic detection,[23] an approach relying on the real-time observation of individual binding events between single substrate molecules and a receptor.[11,24] Protein pores can be selectively functionalized with various probes or aptamers that can bind individual target molecules with high selectivity and sensitivity. The characteristic binding and distinctive current signatures can reveal the identity and concentration of the target analyte[11,25] and can be applied to

earlier disease diagnosis, environmental surveillance, custom quarantines, drug tests, or real-time detection and identification of chemical and biological agents. Additionally, the dynamic interactions between the analyte and the binding sites can be studied in real-time at high resolution using single-channel conductance assays. The channel of the phi29 connector protein has also been embedded into a lipid bilayers inside a microfluidic channel array for detection and sensing purposes.[26]

The translocation of both ssDNA and dsDNA has been studied comprehensively in other biological nanopores, such as the α-hemolysin channel.[27] However, due to the limitations of pore size, modifications of the internal pore of the α-hemolysin channels are difficult. Solid-state nanopores have also been developed during the past decade to detect the translocation of dsDNA and other biomolecules.[28−33] In this report, we present data obtained from a reengineered phi29 connector channel that had an internal loop segment removed from the gp10 subunit. This modification resulted in two subpopulations of channels, each with a different conductance and pore diameter. A group of smaller channels with a conductance of ∼60% of the wild-type connector channels was constructed. These mutant connector channels were able to translocate ssDNA and ssRNA. Moreover, the translocation of ssDNA or ssRNA was observed to be bidirectional. This reengineered connector channel

expands the future applications of phi29 nanopore in nanomedicine and nanobiotechnology.

RESULTS

Reduction of the Size of the Channel by 40% after Deletion of the Internal Channel Loop. The insertion of a single connector channel of the native[20] and modified connector channels[7,18] has been demonstrated. Each type of connector channel exhibits a unique unitary conductance with a sharp Gaussian distribution. Figure 2 shows the overlap of the current traces through individual C-His connector (red) and C-His/Δloop connector channels (blue). The conductance of the channels for wild-type C-His connector channels (red) and C-His/Δloop with the loop deletion (blue) was 4.86 nS (365 pA) and 2.91 nS (218 pA), respectively, in the presence of a conducting buffer composed of 1 M KCl with 5 mM HEPES, pH 7.4. A continuous current recording with multiple C-His/Δloop connector channel insertions was observed (Figure 2B) and analyzed. The histogram for 51 insertion events (Figure 2C) clearly showed that there were two subpopulations of C-His/Δloop connector channels, each with a different unitary conductance. The major peak represents 86% of the C-His/Δloop connector channel insertion events with an average conductance of 2.2 nS. The minor peak represents 8% of the channel insertion events with an average conductance of 3.4 nS. On rare occasions (2% of the cases), two channels were inserted simultaneously into the BLM.

Sensing of Single-Stranded RNA by the Loop-Deleted Channels. Due to the fast speed of translocation and the limit of the instrument sampling frequency, it was difficult to observe the blockade signals for ssDNA or ssRNA translocation through wild-type connector channels. A 20 nt single-stranded 2′-fluoro (2′-F)-modified RNA was used to test the translocation through the modified channel. This particular 20 nt RNA fragment has been shown to have the unusual property of not displaying RNA secondary structure.[34] This oligo cannot be stained by ethidium bromide or SYBR Green,[34] two dyes that are commonly used to detect RNA or DNA by chelating into their double-stranded area. In the absence of ssRNA, no transient changes in the channel currents (spikes) were observed (Figure 3A). After adding 10 nM ssRNA to the BLM cell, spikes appeared after each insertion event, resulting in unique blockade rates after each event (Figure 3B). A schematic illustration of a chamber containing the connector-embedded lipid bilayer is provided in the left inset in Figure 3B, and ssRNA molecules were driven through the channel by the applied electric field (the orientation of the connector channel is for illustrative purpose only). A magnified view reveals an individual signal event representing one ssRNA translocation. Two parameters were used to characterize
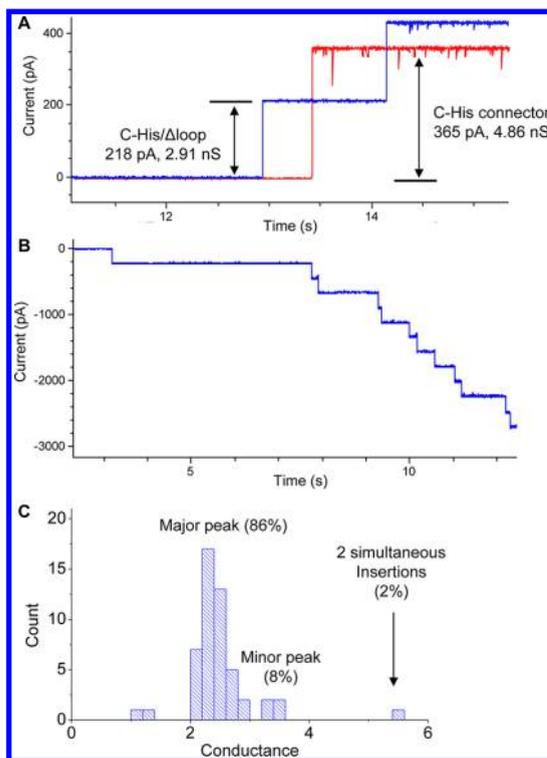

Figure 2. Conductance of the wild-type and mutant connector channel. (A) Current recordings of a typical connector channel composed of C-His gp10 subunits (blue) and a typical connector channel composed of C-His/Δloop gp10 subunits (red). The current trace from C-His gp10 connector channel shows two discrete channel insertions into the BLM. The current trace from the C-His/Δloop gp10 connector channel shows only one channel insertion into the BLM. The current traces were overlaid to display the difference in the unitary channel conductance between the C-His gp10 connector channel and the C-His/Δloop gp10 connector channel. (B) Continuous current recording showing multiple insertions of C-His/Δloop gp10 connector channels. (C) Histogram of C-His/Δloop connector channel conductance for multiple insertion events (n = 51). The plot reveals that there are two subpopulations of C-His/Δloop connector channels, each with a different unitary conductance. The major peak accounts for 86% of the C-His/Δloop connector channel insertion events; these C-his/Δloop connector channels had a conductance of ∼2.2 nS. The minor peak accounts for 8% of channel insertion events; these C-His/Δloop connector channels had a conductance of ∼3.4 nS. In 2% of connector channel insertion events, two channels were inserted simultaneously into the BLM (1 M KCl with 5 mM HEPES, pH 7.4).

these events: dwell time and blockade amplitude. Dwell time is the time the ssRNA takes to translocate through a connector channel and is displayed as the width of a peak. Blockade amplitude is the difference in the current through a channel at baseline and the current during ssRNA translocation, displayed as the amplitude of a peak. The blockade amplitude represents the change in the cross-sectional area of the pore of a connector channel when it is partially occupied by a ssRNA molecule. Histograms of these two parameters from 854 events are shown in Figure 3C,D, respectively. The dwell time under these experimental conditions ranged from 5 to 70 ms, with an average dwell time
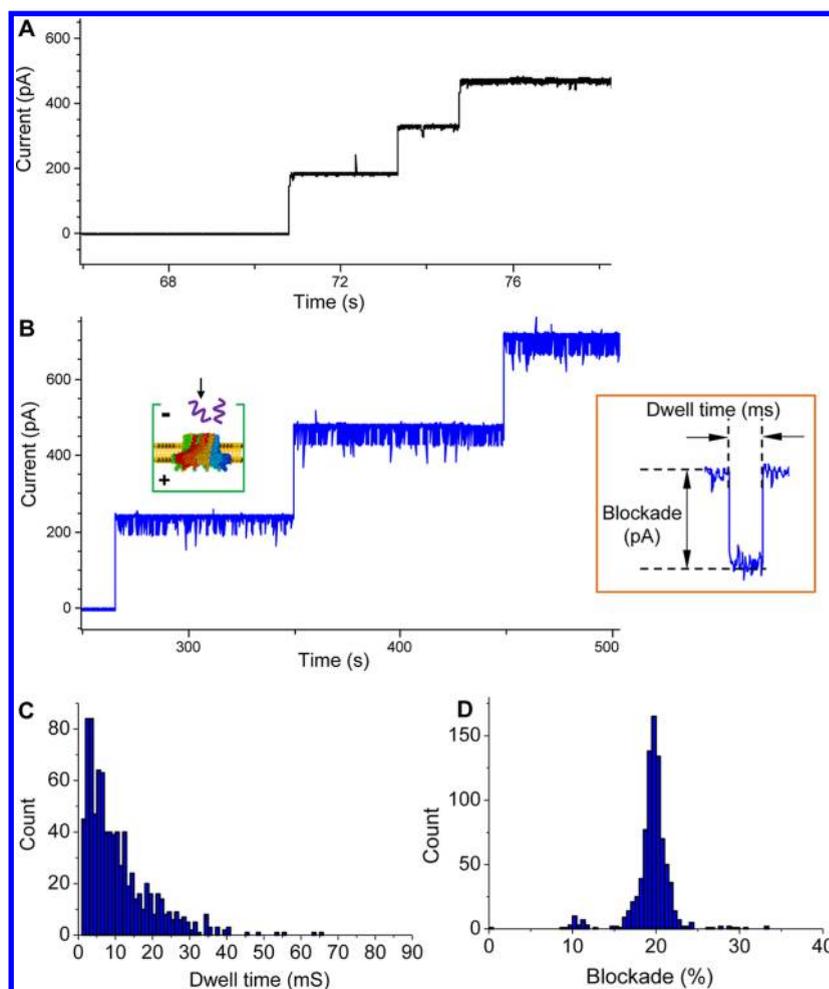
Figure 3. Sensing of ssRNA by the modified channel. (A) Continuous current recording from a control experiment without the addition of ssRNA into the BLM cell. **(B)** Continuous current recording from an experiment with the addition of 2′F ssRNA into the BLM cell. Inset: magnified image of a translocation event. **(C)** Histogram of the dwell time for ssRNA translocation events (*n* = 854). **(D)** Histogram of the blockade amplitude for ssRNA translocation of 854 events (1 M KCl with 5 mM HEPES, pH 7.4, +75 mV applied).

around 15 ms. The histogram of blockade amplitudes revealed an average blockade of 39.3 ± 3.1 pA, representing a blockage of 19.7 ± 2.1% of the loop-deleted channel pore, in contrast to the 31−38% blockage of dsDNA through C-his wild-type pores.[7]

Sensing of Single-Stranded DNA by the Loop-Deleted Channels. Translocation experiments were also performed using a 20 nt single-stranded DNA. The results of these experiments were very similar to the experiments using ssRNA. In the presence of 10 nM ssDNA, a burst of spikes was observed after the incorporation of the modified channel into the BLMs (Figure 4A). Histograms of dwell time and current blockade% from 1191 events are shown in Figure 4C,D, respectively. The dwell time varied from 0.1 to 60 ms (Figure 4B). The average blockade amplitude of the modified connector channel pore was around 39.6 ± 3.6 pA (Figure 4C), representing a blockade of 17.8 ± 1.6% of the modified connector channel pore, which was similar to the blockade% observed for ssRNA.

Bidirectional Translocation of Single-Stranded Nucleic Acids through Loop-Deleted Connector Channels. We previously

reported that dsDNA has a one-way translocation property through C-His-tagged and wild-type connectors.[18,20,22] Electrophysiological measurements with switched polarity and ramping potentials were used to verify the direction of 2′F ssRNA translocation through the channel. When 2′F ssRNA was added to both the top (*cis*) and bottom (*trans*) chambers of the BLM cell, the ssRNA was driven through the channel by the applied voltage potential. With a constant holding potential of +75 mV, blockade events of ssRNA translocation were observed. After switching the polarity to −75 mV, events with a similar blockade percentage were observed (Figure 5A), indicating that ssRNA molecules were able to translocate through both sides of the connector channel pore. The data are in contrast with our previous finding that dsDNA was translocated through the pore in only one direction. Similar bidirectional transport process was observed under a ramping potential of −100 mV to +100 mV (Figure 5B). Moreover, the loop-deleted connectors demonstrated equal translocation capabilities in both directions (Figure 5B).
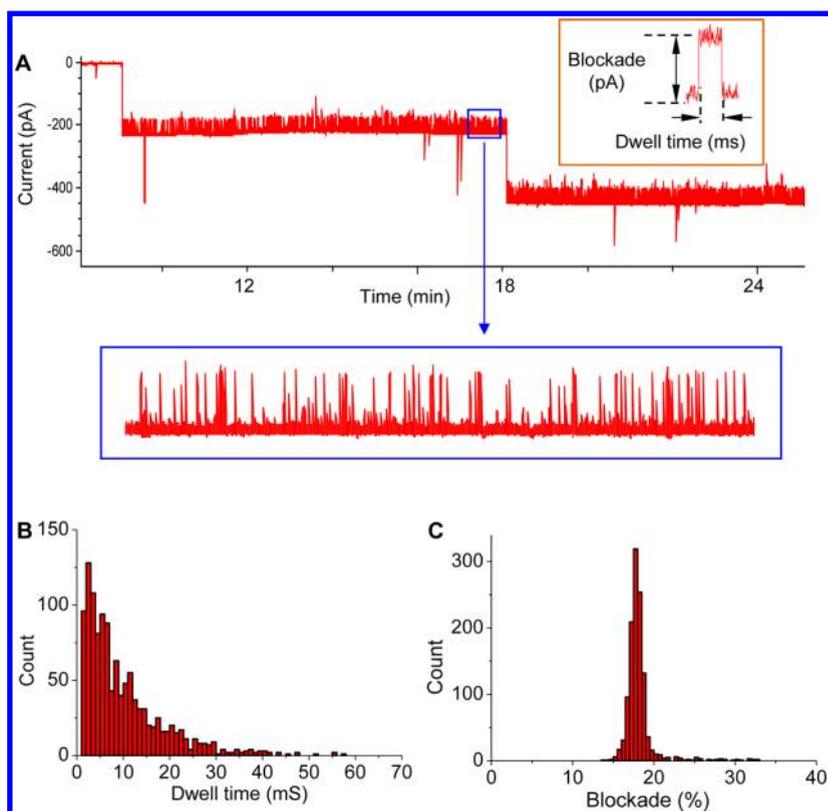
Figure 4. Sensing of ssDNA by the modified channel. (A) Continuous current recording from an experiment with the addition of ssDNA into the BLM cell. Inset: magnified multiple ssDNA translocation events and a single translocation event. **(B)** Histogram of the dwell time for ssDNA translocation events (*n* = 1191). **(C)** Histogram of the blockade amplitude for ssDNA translocation of the 1191 events (1 M KCl with 5 mM HEPES, pH 7.4, −75 mV applied).
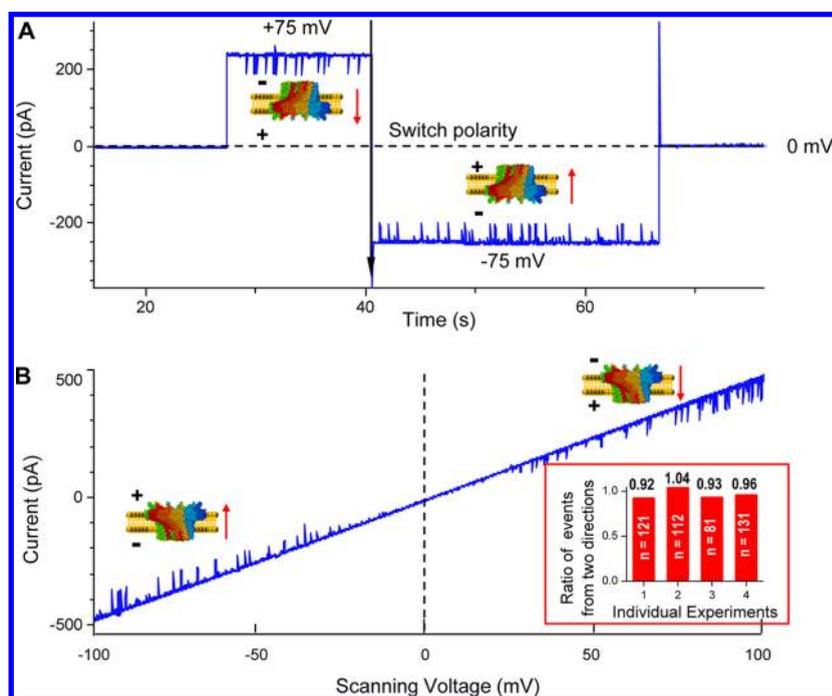

Figure 5. Bidirectional translocation of the ssRNA. (A) Continuous current recording during a switch in the polarity of constant holding potential. The ssRNA translocation events at +75 mV produced downward spikes, while the translocation events at −75 mV produced upward spikes. **(B)** Continuous current recording during a ramping potential from −100 mV to +100 mV. The spikes representing ssRNA translocation events switched from upward deflections to downward deflections. Inset: Ratio of forward and reverse ssRNA translocation events (1 M KCl with 5 mM HEPES, pH 7.4).
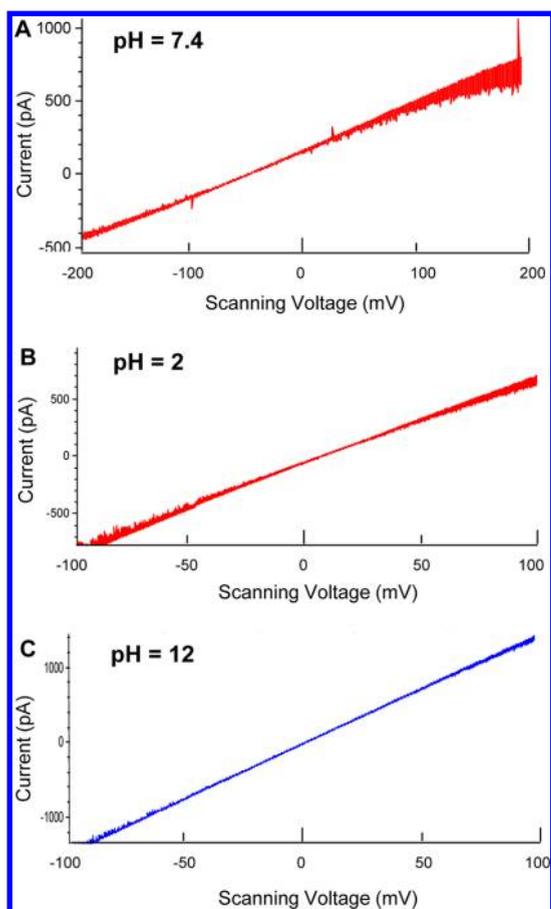
Figure 6. Stability of the modified channel at various conditions. (A) High ramping potential at pH 7.4. (B) Acidic buffer condition of pH 2. (C) Alkaline buffer condition of pH 12.

Stability Assay of the Loop-Deleted Channels under Different pH and Voltage Conditions. The gating property of the connector channel at higher potentials (>100 mV) has been observed in several mutants.[19] However, in order for the connector channels to be useful for a wide variety of applications, the connector channels must be stable at high potentials and extreme pH environments. Accordingly, the stability of the loop-deleted connector channel was examined under high voltages (±200 mV) (Figure 6A). At constant holding potentials (±200 mV), the channels were found to be quite stable, while the wild-type C-His connector had been shown to gate immediately.[19] Similar results were observed under a ramping potential (−200 mV to +200 mV, 1 M KCl with 5 mM HEPES, pH 7.4). The loop-deleted connectors were also stable at extreme pH environments, as demonstrated by linear current−voltage trace at pH 2 (5 mM H_3PO_4 buffer) and pH 12 (5 mM Na_2H-$PO_4 \cdot 7H_2O$ buffer) (Figure 6B,C).

DISCUSSION

Various modifications have been studied extensively on both biological nanopores and solid-state nanopores for use in nucleic acid sensing.[24,35] The modification of biological nanopores can be easily achieved by the insertion, deletion, or substitution of various amino acids.[20,36] Biological nanopores can also be modified by covalently linking molecular recognition agents in the interior lumen of the pores.[11] Solid-state nanopores, conversely, have been studied mainly by chemical modifications. Different assembly pathways from modified phage portal protein monomers have been reported on SPP1,[37] phi29,[4] T7,[38] and P2.[39] Both 12-mer and 13-mer assemblies of SPP1 connectors were obtained at different conditions.[37] The mutations and modifications of these portal protein channels can be used to investigate and refine the nanopores for technical applications, such as DNA sequencing.

The C-His/Δloop mutation in the gp10 subunit protein resulted in the production of two subpopulations of connector channels: a small proportion of the channels had a conductance similar to the channels of wild-type gp10 subunits, while the vast majority had a conductance of ∼60% of the wild-type (Figure 2A). The former subpopulation of connector channels may have a structure similar to the dodecameric wild-type connector channels. The subpopulation of connector channels with smaller conductance may have a different structure, possibly composed of fewer subunits. It should also be noted that both types of channels were observed from the same batch of mutant gp10 protein subunit. To avoid possible contamination, three-generation single-colony purification was carried out. The purified C-His/Δloop connector channels from different batches showed similar results (Figure 1C). While the two subpopulations of connector channels had a different channel size, both of them could be incorporated into the bilayer, indicating that the outer surface charge and hydrophilicity was not affected by the deletion of internal flexible loops. The conductance (G) of a nanopore can be simplified as a cylindrical pore and calculated using the equation: $G = (\sigma \pi d^2)/4l$, where σ is the conductivity of the buffer solution, d represents pore diameter, and l represents pore length. Since the wild-type connector channel has an internal pore diameter of 3.6 nm, the pore diameter of the smaller mutant channel can be estimated to be ∼2.78 nm. This reduction in the pore size contributes to the improved signal-to-noise ratio and allows more precious sensing for single-stranded nucleic acid molecules.

Translocation of single-stranded DNA or RNA by biological or solid-state nanopores has drawn great attention and has been well-studied in recent years by several research groups because of its importance in DNA sequencing and many other applications.[40−43] Discrimination between single- and double-stranded nucleic acid molecules by translocating single-stranded homopolymers poly (A), poly (U), and poly (C) through solid-state nanopores has been reported.[40] The translocation of long random sequences and short length ssDNA through solid-state nanopores has been characterized and compared with the dsDNA and the hybrid

DNA/RNA.[41,42] The relatively large diameter of the connector channel is an ideal tool for studying dsDNA transport,[7] but detection of single-stranded nucleic acids remains difficult using the system reported previously.[7,8] In this paper, we generated smaller connector channels by deleting the internal loop segments of gp10 subunits and demonstrated their capability to detect ssDNA and ssRNA. The translocation events produced a uniform current blockade of 16−21%, with a peak value of ~19%. This blockade percentage is approximately half of the dsDNA blockade through the native channel, even though the cross-sectional area of the mutant channel is only 60% of the wild-type.

Most solid-state nanopores have little selectivity on the direction of DNA and RNA transport.[44] The one-way traffic mechanism in the phi29 viral nanomotor connector protein channel showed an intriguing and sophisticated controlled transport of nucleic acids. The purified wild-type connector protein retains the one-way traffic property for the dsDNA translocation *in vitro*.[18,20,22,45] Enthrallingly, the C-His/Δloop mutant connector can translocate the ssDNA or ssRNA from both directions (Figure 5). The gating behaviors for both wild-type and C-His/Δloop mutant have been studied and compared,[19] and the results suggest that the internal flexible loop in the internal lumen may play a key role in the stepwise closing and reopening of the channel. In four independent experiments, the ratio of number of events for translocation from *cis*-chamber and *trans*-chamber was close to 1:1 (ranged from 0.92 to 1.04:1) (Figure 5B inset), indicating that there is no selectivity for the passive translocation of single-stranded nucleic acid molecules through the loop-cleaved connector channel. The underlying mechanism of one-way traffic property of the connector channel is still under investigation.

CONCLUSION

The deletion of an internal flexible segment from the gp10 subunit of the phi29 DNA-packaging nanomotor resulted in a smaller conductance channel with a pore diameter ~60% of the wild-type connector channel. While the single-stranded nucleic acids could not be detected by wild-type channel, they showed a blockade of 16−21% while being translocated through the smaller size channel. This mutant channel with smaller size is ideal for the detection and sensing of single-stranded nucleic acids, including ssDNA and ssRNA. Connector channels created from gp10 subunits with the internal loop deleted allowed for bidirectional translocation of single-stranded nucleic acids. This may also lead to the development of a hybrid system in which the smaller conductance channel can be reconstituted into a lipid bilayer, in conjunction with the wild-type connector channel, for the simultaneous detection and sensing of both dsDNA and ssDNA.

MATERIALS AND METHODS

Materials. The phospholipids 1,2-diphytanoyl-*sn*-glycerol-3-phosphocholine (DPhPC) and 1,2-dioleoyl-*sn*-glycerol-3-phosphocholine (DOPC) were obtained from Avanti Polar Lipids, Inc. Organic solvents (*n*-decane and chloroform) were purchased from Fisher Scientific, Inc. and TEDIA, Inc., respectively. The DNA and RNA oligonucleotides used in this study were obtained from Integrated DNA Technologies, Inc. All other reagents were purchased from Sigma-Aldrich, Inc. if not specified.

Cloning and Purification of the Phi29 Connector Protein. Two mutant versions of the connector subunit protein were used in this research: a connector subunit with the C-terminus tagged with 14 histidine (His) residues (C-His gp10) and a connector subunit with the same C-terminus His tag and the internal flexible loop removed (C-His/Δloop gp10) (Figure 1C). The cloning, expression, and purification of these C-His connector protein subunits have been previously reported,[7,9,20] as well as the construction of the C-His/Δloop connector.[19]

The connector mutants were expressed in *Escherichia coli* and purified by nickel affinity chromatography.[13] Pelleted cells were resuspended with His binding buffer (15% glycerol, 0.5 M NaCl, 5 mM imidazole, 10 mM ATP, 50 mM Na_2HPO_4/NaH_2PO_4, pH 8.0), and the cleared lysate was loaded onto a His·Bind resin column (Novagen) and washed with His wash buffer (15% glycerol, 0.5 M NaCl, 50 mM imidazole, 10 mM ATP, 50 mM Na_2HPO_4/NaH_2PO_4, pH 8.0). The His-tagged connector protein subunits were eluted from the column with His elution buffer (15% glycerol, 0.5 M NaCl, 0.5 M imidazole, 50 mM ATP, 50 mM Na_2HPO_4/NaH_2PO_4, pH 8.0).

Incorporation of the Connector Channels into Giant Liposomes. Liposomes containing the connector channels were prepared following the procedure of recent reports.[7,8,17−19] Briefly, a dehydration and rehydration procedure was used to form giant unilammellar vesicles (GUVs), with an average diameter of 50 μm. The connector channels were mixed with DOPC at the rehydration stage, during which the DOPC was coincubated with the connector protein in sucrose buffer (1 M NaCl, 200 mM sucrose, 10 mM Tris, pH 7.9). The lipid solution was then passed through a polycarbonate membrane filter (100 or 400 nm) to generate GUVs. The formation of the vesicles was observed by bright-field microscopy. The final molar ratio of lipids to connector proteins was in the range of 4000:1 to 16000:1 in the GUVs.

Insertion of the Connector Protein into Preformed Lipid Bilayers. Procedures have been recently developed[7,8,17−19] for the incorporation of connector channels into lipid bilayers. Planar bilayer lipid membranes (BLMs) were created in a BCH-1A horizontal BLM cell (Eastern Scientific, LLC). A Teflon partition with a 0.2 mm aperture was placed in the apparatus to separate the top and bottom compartments of the BLM cell. A planar lipid bilayer of DPhPC was formed by painting the aperture with 0.5 μL of 3% (w/v) DPhPC in *n*-decane. A conducting buffer (1 M NaCl, 10 mM Tris-HCl, pH 7.8) was added to both the top and bottom compartments of the BLM cell, and a Ag/AgCl electrode was placed in the buffer of each compartment. The electrode in the bottom compartment was connected to the headstage of an Axopatch 200B amplifier (Axon Instruments, Inc.), and the electrode in the top compartment was grounded.

When a planar BLM was successfully formed in the aperture of the partition, separating the two compartments filled with buffer, the BLM acted as an insulator. Intact planar BLM exhibited no detectable electrical current between the two electrodes. GUVs (0.5−2.0 μL) containing connector channels were added to the top compartment. Membrane fusion between the liposomes and the BLM happened immediately after applying GUVs containing the connector protein, and it was found that a current passing through the connector channel could be recorded.

Electrophysiological Measurements. The headstage and Axopatch 200B patch clamp amplifier were connected to a DigiData 1440 analog−digital converter (Axon Instruments, Inc.) to monitor and record electrochemical currents through BLMs.[7,8,17] The current recordings were low-pass filtered at a frequency of 1 kHz. The sampling frequency was 2 kHz in all experiments, unless otherwise specified. The data were recorded and stored on a PC with pClamp 9.1 software (Axon Instruments, Inc.) and analyzed with the Clampfit module of pClamp 9.1 and OriginPro 8.1 (OriginLab Corporation).

Electrical potentials were applied across BLMs in experiments with two different modes, holding potential mode and ramping potential mode with the pClamp 9.1 software. The ramping potential mode was used in the experiments to examine connector channel stability and DNA/RNA translocation orientation. In the holding potential mode, a constant voltage (either +75 mV or −75 mV) was applied across the BLM. In the ramping potential mode, a voltage which constantly increased over time, from either −100 mV or +100 mV to −200 mV or +200 mV, was applied across the BLM.

Purification of the DNA/RNA Used in the Experiment. A synthetic 20 nt DNA fragment was purified by mixing a 100 μM stock of the oligonucleotide with an equal volume of 2× TBE buffer (178 mM Tris base, 178 mM boric acid, 2 mM EDTA, pH 8.3). The oligonucleotide/TBE mixture was loaded onto an 8% (w/v) polyacrylamide gel containing 8 M urea−TBE. The DNA was electrophoresed through the gel at 120 V for ∼1 h. After electrophoresis, the single-stranded DNA band was visualized as a shadow on a TLC plate with a hand-held UV light and then cut out of the gel. The gel containing the ssDNA was minced, and the ssDNA was eluted from the gel fragments by incubation in a small volume of elution buffer (0.5 M ammonium acetate) at 37 °C for 4 h. The gel fragments were pelleted by centrifugation, and the supernatant was removed. The ssDNA was precipitated from the supernatant by adding 1/10 volume of 3 M sodium acetate and 2.5 volumes of ethanol and storing the solution overnight at −20 °C. The ssDNA was again pelleted by centrifugation, and excess salt was removed by rinsing the ssDNA pellet with 70% ethanol. The purified ssDNA was dissolved and stored in TMS buffer (100 mM NaCl, 10 mM MgCl$_2$, 50 mM Tris-HCl, pH 8.0). A synthetic 20 nt ssRNA fragment was purified in a similar manner.

Translocation Experiments of DNA and RNA. Liposomes containing connector channels were added to the top compartment of the BLM cell. Soon after, highly conductive connector channel(s) were inserted into the planar BLM, and a stepwise increase in current was observed. For translocation experiments, the purified ssDNA or ssRNA was mixed with conducting buffer and added to the top compartment in the BLM cell. The translocation of ssDNA or ssRNA was observed as transient blockades of the electrochemical current.

REFERENCES AND NOTES

1. Guo, P. Structure and Function of Phi29 Hexameric RNA That Drive Viral DNA Packaging Motor: Review. *Prog. Nucleic Acid Res. Mol. Biol.* **2002**, *72*, 415–472.
2. Guo, P. X.; Lee, T. J. Viral Nanomotors for Packaging of dsDNA and dsRNA. *Mol. Microbiol.* **2007**, *64*, 886–903.
3. Simpson, A. A.; Leiman, P. G.; Tao, Y.; He, Y.; Badasso, M. O.; Jardine, P. J.; Anderson, D. L.; Rossman, M. G. Structure Determination of the Head-Tail Connector of Bacteriophage Phi29. *Acta Crystallogr.* **2001**, *D57*, 1260–1269.
4. Guasch, A.; Pous, J.; Ibarra, B.; Gomis-Ruth, F. X.; Valpuesta, J. M.; Sousa, N.; Carrascosa, J. L.; Coll, M. Detailed Architecture of a DNA Translocating Machine: The High-Resolution Structure of the Bacteriophage Phi29 Connector Particle. *J. Mol. Biol.* **2002**, *315*, 663–676.
5. Lee, C. S.; Guo, P. Sequential Interactions of Structural Proteins in Phage Phi29 Procapsid Assembly. *J. Virol.* **1995**, *69*, 5024–5032.
6. Fu, C.; Prevelige, P. *In Vitro* Incorporation of the Phage Phi29 Connector Complex. *Virology* **2009**, *394*, 149–153.
7. Wendell, D.; Jing, P.; Geng, J.; Subramaniam, V.; Lee, T. J.; Montemagno, C.; Guo, P. Translocation of Double-Stranded DNA Through Membrane-Adapted Phi29 Motor Protein Nanopores. *Nat. Nanotechnol.* **2009**, *4*, 765–772.
8. Jing, P.; Haque, F.; Vonderheide, A.; Montemagno, C.; Guo, P. Robust Properties of Membrane-Embedded Connector Channel of Bacterial Virus Phi29 DNA Packaging Motor. *Mol. Biosyst.* **2010**, *6*, 1844–1852.
9. Cai, Y.; Xiao, F.; Guo, P. The Effect of N- or C-Terminal Alterations of the Connector of Bacteriophage Phi29 DNA Packaging Motor on Procapsid Assembly, PRNA Binding, and DNA Packaging. *Nanomedicine* **2008**, *4*, 8–18.
10. Guo, Y.; Blocker, F.; Xiao, F.; Guo, P. Construction and 3-D Computer Modeling of Connector Arrays with Tetragonal to Decagonal Transition Induced by PRNA of Phi29 DNA-Packaging Motor. *J. Nanosci. Nanotechnol.* **2005**, *5*, 856–863.
11. Haque, F.; Lunn, J.; Fang, H.; Smithrud, D.; Guo, P. Real-Time Sensing and Discrimination of Single Chemicals Using the Channel of Phi29 DNA Packaging Nanomotor. *ACS Nano* **2012**, *6*, 3251–3261.
12. Ibanez, C.; Garcia, J. A.; Carrascosa, J. L.; Salas, M. Overproduction and Purification of the Connector Protein of *Bacillus subtilis* Phage Φ29. *Nucleic Acids Res.* **1984**, *12*, 2351–2365.
13. Robinson, M. A.; Wood, J. P.; Capaldi, S. A.; Baron, A. J.; Gell, C.; Smith, D. A.; Stonehouse, N. J. Affinity of Molecular Interactions in the Bacteriophage Phi29 DNA Packaging Motor. *Nucleic Acids Res.* **2006**, *34*, 2698–2709.
14. Xiao, F.; Sun, J.; Coban, O.; Schoen, P.; Wang, J. C.; Cheng, R. H.; Guo, P. Fabrication of Massive Sheets of Single Layer Patterned Arrays Using Lipid Directed Reengineered Phi29 Motor Dodecamer. *ACS Nano* **2009**, *3*, 100–107.
15. Xiao, F.; Cai, Y.; Wang, J. C.; Green, D.; Cheng, R. H.; Demeler, B.; Guo, P. Adjustable Ellipsoid Nanoparticles Assembled from Re-engineered Connectors of the Bacteriophage Phi29 DNA Packaging Motor. *ACS Nano* **2009**, *3*, 2163–2170.
16. Xiao, F.; Demeler, B.; Guo, P. Assembly Mechanism of the Sixty-Subunit Nanoparticles *via* Interaction of RNA with the Reengineered Protein Connector of Phi29 DNA-Packaging Motor. *ACS Nano* **2010**, *4*, 3293–3301.
17. Haque, F.; Geng, J.; Montemagno, C.; Guo, P. Incorporation of Viral DNA Packaging Motor Channel in Lipid Bilayers for Real-Time, Single-Molecule Sensing of Chemicals and Double-Stranded DNA. *Nat. Protoc.* **2013**, *8*, 373–392.
18. Jing, P.; Haque, F.; Shu, D.; Montemagno, C.; Guo, P. One-Way Traffic of a Viral Motor Channel for Double-Stranded DNA Translocation. *Nano Lett.* **2010**, *10*, 3620–3627.
19. Geng, J.; Fang, H.; Haque, F.; Zhang, L.; Guo, P. Three Reversible and Controllable Discrete Steps of Channel Gating of a Viral DNA Packaging Motor. *Biomaterials* **2011**, *32*, 8234–8242.
20. Fang, H.; Jing, P.; Haque, F.; Guo, P. Role of Channel Lysines and "Push through a One-Way Valve" Mechanism of Viral DNA Packaging Motor. *Biophys. J.* **2012**, *102*, 127–135.
21. Grimes, S.; Ma, S.; Gao, J.; Atz, R.; Jardine, P. J. Role of Phi29 Connector Channel Loops in Late-Stage DNA Packaging. *J. Mol. Biol.* **2011**, *410*, 50–59.
22. Zhang, H.; Schwartz, C.; De Donatis, G. M.; Guo, P. "Push through One-Way Valve" Mechanism of Viral DNA Packaging. *Adv. Virus Res.* **2012**, *83*, 415–465.
23. Bayley, H.; Cremer, P. S. Stochastic Sensors Inspired by Biology. *Nature* **2001**, *413*, 226–230.
24. Haque, F.; Li, J.; Wu, H.-C.; Liang, X.-J.; Guo, P. Solid-State and Biological Nanopore for Real-Time Sensing of Single

Chemical and Sequencing of DNA. *Nano Today* **2013**, *8*, 56–74.

25. Geng, J.; Vonderheide, A. Versatile DNA-Packaging Nano-motor of Bacteriophage Phi29 with Applications in Nano-biotechnology. *Nano LIFE* **2010**, *1*, 45–62.

26. Shim, J. S.; Geng, J.; Ahn, C. H.; Guo, P. Formation of Lipid Bilayers Inside Microfluidic Channel Array for Monitoring Membrane-Embedded Nanopores of Phi29 DNA Packaging Nanomotor. *Biomed. Microdevices* **2012**, *14*, 921–928.

27. Tobkes, N.; Wallace, B. A.; Bayley, H. Secondary Structure and Assembly Mechanism of an Oligomeric Channel Protein. *Biochemistry* **1985**, *24*, 1915–1920.

28. Storm, A. J.; Chen, J. H.; Ling, X. S.; Zandbergen, H. W.; Dekker, C. Fabrication of Solid-State Nanopores with Single-Nanometre Precision. *Nat. Mater.* **2003**, *2*, 537–540.

29. Li, J.; Gershow, M.; Stein, D.; Brandin, E.; Golovchenko, J. A. DNA Molecules and Configurations in a Solid-State Nano-pore Microscope. *Nat. Mater.* **2003**, *2*, 611–615.

30. Smeets, R. M. Salt Dependence of Ion Transport and DNA Translocation through Solid-State Nanopores. *Nano Lett.* **2006**, *6*, 89–95.

31. Wanunu, M.; Meller, A. Chemically-Modified Solid-State Nanopores. *Nano Lett.* **2007**, *7*, 1580–1585.

32. Wanunu, M.; Sutin, J.; McNally, B.; Chow, A.; Meller, A. DNA Translocation Governed by Interactions with Solid State Nanopores. *Biophys. J.* **2008**, *95*, 4716–4725.

33. Wei, R.; Gatterdam, V.; Wieneke, R.; Tampe, R.; Rant, U. Stochastic Sensing of Proteins with Receptor-Modified Solid-State Nanopores. *Nat. Nanotechnol.* **2012**, *7*, 257–263.

34. Shu, D.; Shu, Y.; Haque, F.; Abdelmawla, S.; Guo, P. Thermo-dynamically Stable RNA Three-Way Junctions for Con-structing Multifuntional Nanoparticles for Delivery of Therapeutics. *Nat. Nanotechnol.* **2011**, *6*, 658–667.

35. Venkatesan, B. M.; Bashir, R. Nanopore Sensors for Nucleic Acid Analysis. *Nat. Nanotechnol.* **2011**, *6*, 615–624.

36. Braha, O.; Walker, B.; Cheley, S.; Kasianowicz, J. J.; Song, L.; Gouaux, J. E.; Bayley, H. Designed Protein Pores as Com-ponents for Biosensors. *Chem. Biol.* **1997**, *4*, 497–505.

37. Lebedev, A. A.; Krause, M. H.; Isidro, A. L.; Vagin, A. A.; Orlova, E. V.; Turner, J.; Dodson, E. J.; Tavares, P.; Antson, A. A. Structural Framework for DNA Translocation *via* the Viral Portal Protein. *EMBO J.* **2007**, *26*, 1984–1994.

38. Agirrezabala, X.; Martin-Benito, J.; Valle, M.; Gonzalez, J. M.; Valencia, A.; Valpuesta, J. M.; Carrascosa, J. L. Structure of the Connector of Bacteriophage T7 at 8Å Resolution: Structural Homologies of a Basic Component of a DNA Translocating Machinery. *J. Mol. Biol.* **2005**, *347*, 895–902.

39. Cingolani, G.; Moore, S. D.; Prevelige, J.; Johnson, J. E. Preliminary Crystallographic Analysis of the Bacterioph-age P22 Portal Protein. *J. Struct. Biol.* **2002**, *139*, 46–54.

40. Skinner, G. M.; van den Hout, M.; Broekmans, O.; Dekker, C.; Dekker, N. H. Distinguishing Single- and Double-Stranded Nucleic Acid Molecules Using Solid-State Nanopores. *Nano Lett.* **2009**, *9*, 2953–2960.

41. Kowalczyk, S. W.; Tuijtel, M. W.; Donkers, S. P.; Dekker, C. Unraveling Single-Stranded DNA in a Solid-State Nano-pore. *Nano Lett.* **2010**, *10*, 1414–1420.

42. Mathe, J.; Aksimentiev, A.; Nelson, D. R.; Schulten, K.; Meller, A. Orientation Discrimination of Single-Stranded DNA Inside the α-Hemolysin Membrane Channel. *Proc. Natl. Acad. Sci. U.S.A.* **2005**, *102*, 12377–12382.

43. Kawano, R.; Schibel, A. E. P.; Cauley, C.; White, H. S. Con-trolling the Translocation of Single-Stranded DNA through α-Hemolysin Ion Channels Using Viscosity. *Langmuir* **2008**, *25*, 1233–1237.

44. Branton, D.; Deamer, D. W.; Marziali, A.; Bayley, H.; Benner, S. A.; Butler, T.; Di, V. M.; Garaj, S.; Hibbs, A.; Huang, X.; *et al.* The Potential and Challenges of Nanopore Sequencing. *Nat. Biotechnol.* **2008**, *26*, 1146–1153.

45. Zhao, Z.; Khisamutdinov, E.; Schwartz, C.; Guo, P. Mecha-nism of One-Way Traffic of Hexameric Phi29 DNA Packaging Motor with Four Electropositive Relaying Layers Facilitat-ing Anti-parallel Revolution. *ACS Nano* Submitted for publication.